PROCEEDINGS REPRINT

SPIE—The International Society for Optical Engineering

Reprinted from

Space Processing of Materials

4–5 August 1996
Denver, Colorado

Volume 2809

©1996 by the Society of Photo-Optical Instrumentation Engineers
Box 10, Bellingham, Washington 98227 USA. Telephone 360/676-3290.

NASA-CR-204586

Convective influence on radial segregation during unidirectional solidification of the binary alloy HgCdTe

D.A. Watring, D.C. Gillies, S.L. Lehoczky, F.R. Szofran

Space Sciences Laboratory
Marshall Space Flight Center, Huntsville, Alabama 35812

H. Alexander
Universities Space Research Association, Huntsville, Alabama 35806

ABSTRACT

In order to simulate the space environment for basic research into the crystal growth mechanism, $Hg_{0.8}Cd_{0.2}Te$ crystals were grown by the vertical Bridgman-Stockbarger method in the presence of an applied axial magnetic field. The influence of convection, by magneto hydrodynamic damping, on mass transfer in the melt and segregation at the solid-liquid interface was investigated by measuring the axial and radial compositional variations in the grown samples. The reduction of convective mixing in the melt through the application of the magnetic field is found to have a large effect on radial segregation and interface morphology in the grown crystals. Direct comparisons are made with a $Hg_{0.8}Cd_{0.2}Te$ crystal grown without field and also in the microgravity environment of space during the second United States Microgravity Payload Mission (USMP-2).

1 Introduction

The Hg based II-VI semiconductor, $Hg_{1-x}Cd_xTe$, is important for application of infrared detection and imaging applications. Its band gap, E_g, varies linearly with composition, x,

$$E_g = 1.9x - 0.3 \tag{1}$$

which allows it to be compositionally tuned for a broad range of wavelengths from 0.8 μm to the far-infrared spectrum beyond 30 μm. Due to the high Hg vapor pressure present during the processing of this material it must be sealed in a thick silica ampoule. This causes a large destabilizing horizontal temperature gradient to be generated due to a difference in the thermal conductivities of the melt and crystal and the release of latent heat at the growth interface in the presence of the silica ampoules as predicted by Jasinski and Witt.[1] Additionally, a stabilizing vertical solutal gradient is produced by the rejection of the denser solute, $HgTe$, in to the melt. These phenomena, coupled with a large solutal-to-thermal expansion coefficient

$$\frac{\beta_s C_0}{\beta_t \Delta T} \approx 100 \tag{2}$$

0-8194-2197-9/96/$6.00

and a large thermal-to-solutal diffusion coefficient ratio

$$\frac{\alpha}{D} \approx 200, \tag{3}$$

give rise to double diffusive convection during melt growth. This buoyant convection, due to fluid density differences which are often small, can produce strong convection in all noncapillary solidification processes. The equation which determines the intensity of convection is the Navier-Stokes (N-S) or momentum equation,

$$\rho \frac{D\vec{V}}{Dt} = -\nabla P + \mu \nabla^2 \vec{V} + \rho \vec{G}. \tag{4}$$

Expanding equation 4 in the x direction with the Boussinesq approximation for the density dependence on temperature and solute concentration yields,

$$\rho\left[\frac{\partial V_x}{\partial t} + V_x \frac{\partial V_x}{\partial x} + V_y \frac{\partial V_x}{\partial y}\right] = -\frac{\partial P}{\partial x} + \mu\left[\frac{\partial^2 V_x}{\partial x^2} + \frac{\partial^2 V_x}{\partial y^2}\right] + \rho g \beta_t (\Delta T) + \rho g \beta_s (\Delta C) \tag{5}$$

where ρ is the fluid density and μ is the fluid viscosity, g is the acceleration due to gravity, β_t is the thermal expansion coefficient, β_s is the solutal expansion coefficient, ΔT is the driving temperature difference and ΔC is the driving solutal difference. This equation is nothing more than Newtons first law:

$$M \frac{D\vec{V}}{Dt} = \sum \vec{F} \tag{6}$$

i.e., the summation of forces are equal to the product of an objects mass, M, and acceleration, $\frac{D\vec{V}}{Dt}$, derived for an elemental fluid volume. Therefore, every term in the N-S equation is merely a force. The driving temperature difference, ΔT, in the thermal buoyant force is determined by the energy equation:

$$\rho C_p \frac{DT}{Dt} = K \nabla^2 T \tag{7}$$

where ρ is the density, C_p is the specific heat at constant pressure and K is the thermal conductivity. Similarly, the driving solutal difference, ΔC, in the solutal force is determined by the species equation:

$$\frac{DC}{Dt} = D \nabla^2 C \tag{8}$$

where D is the solutal diffusivity.

During crystal growth, the severity of convection is governed by the highly coupled form of equations 4, 7 and 8. Namely, ratio of the thermal and solutal buoyant forces to the viscous forces. The ratio of these forces is given by a dimensionless parameter known as the Grashof number, Gr,

$$Gr_t = \frac{g \beta_T \Delta T L^3}{\nu^2} \quad and \quad Gr_s = \frac{g \beta_s \Delta C L^3}{\nu^2} \tag{9}$$

where L^3 is the characteristic length scale of the system (for vertical Bridgman-Stockbarger growth the length scale is the crystal radius, r_{cr}), ν is the kinematic viscosity and α is the thermal diffusivity. The subscripts, t and s, denote thermal and solutal respectively.

As mentioned previously, the thermal force is due to density differences arising from unavoidable radial temperature gradients in the melt which promote convection. Solutal forces are due to density differences due to the rejection of solute during solidification. In dilute alloys the solute rejection has little influence on density and the Gr_s is small compared to the Gr_t. However, in nondilute alloys such as $Hg_{1-x}Cd_xTe$ this solutal force is significant and has a large effect on the fluid flow intensity and fluid flow pattern in the melt which can, in turn, have a significant effect on crystal composition. This is easily seen from equation 1. A few percent change in composition, x, will dramatically change the samples bandgap, E_g.

1.1 Methods to Reduce Segregation

It has been shown that fluid flow can interfere with segregation and lead to the nonuniform incorporation of conservative and nonconservative dopants into the grown crystal. If the dopant distribution is not radially uniform within a few percent the material is useless to device manufacturers. In order to control convection and segregation in the material, the growth system parameters such as charge size, temperature gradients and acceleration due to gravity must be modified. Through, for example, growing small diameter crystals, processing in space or under the influence of applied magnetic fields.

1.1.1 Reduction of Charge Diameter

As the severity of convection in crystal growth from the melt is controlled by the Grashof number shown in equation 9 which has a cubic dependence on the crystal radius, r_{rc}, the radius is one of the obvious parameters to change in order to reduce convection. To this end, experiments were performed with various charge diameters during vertical Bridgman growth of Ga-doped Ge.[2] Results showed that the crystal diameter had to be reduced to capillary size to avoid convection in the melt. Obviously, capillary sized crystals are of no value to the electronic industry. They have, however, been found useful for important studies of the semiconductor's thermophysical properties such as diffusion coefficient measurements.

1.1.2 Reduction of Gravity

Another parameter which can be used to control convection is the acceleration due to gravity, g. Experiments[3]$-$[8] performed in the reduced gravity environment of space have shown that diffusion limited growth can be obtained. The real advantage of processing in microgravity is that it provides the opportunity to grow larger diameter crystals in the diffusion limited regime than is possible on earth. This can be readily shown through scaling analysis by comparing the convective acceleration force to the thermal driving force. This relationship is shown in figure 1a as the Reynolds number, Re,

$$Re = \frac{V r_{rc}}{\nu} \tag{10}$$

verses the Grashof number, Gr_t. Multiplying the Re by the Prandtl number, $Pr = \frac{\nu}{\alpha}$, for the first case, and by the Schmidt number, $Sc = \frac{\nu}{D}$, for the second case, yields plots similar to figure 1a where $(RePr) = Pe_t$ and $(ReSc) = Pe_s$. Noting that

$$\frac{Pe_t}{Pe_s} = \frac{D}{\alpha} = 10^{-3} \tag{11}$$

for typical semiconductors, a Re of 10 in figure 1a becomes a Pe_t of 0.1 and a Pe_s of 100 in figures 1b and 1c respectively.

These figures show that diffusion limited heat transfer ($Pe_t < 1$) can be obtained at high values of g (say on earth) and at the same g-level have convection dominated mass transfer ($Pe_s > 1$). Therefore, to get diffusion limited mass transfer the Gr_t (g-level) has to be reduced to very low levels such that $Pe_s < 1$, at which point Pe_t is very small (recall: the ratio of the two was 10^{-3}). It can be shown that the functional dependence of Pe_s on Gr_t is

$$Pe_s = \frac{V r}{\nu}\frac{\nu}{D} \approx fcn\left(\frac{g\beta_s \Delta C r^3}{\nu^2}, Pr, Sc\right). \tag{12}$$

The quantities $\beta, \Delta T, \nu, \alpha$ are fixed for a given crystal growth system and on earth g is fixed which leaves the crystal radius as the only adjustable parameter. However, in space one can lower g easily by four orders of

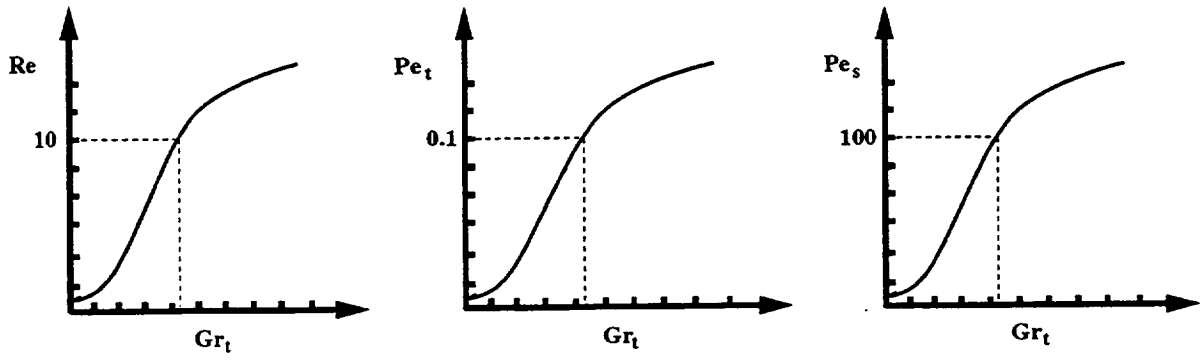

Figure 1: (a) Plot of Re vs. Gr_t , (b) Plot of Pe_t vs. Gr_t, (c) Plot of Pe_s vs. Gr_t for a typical semiconductor material.

magnitude. Thus, from equation 12 (roughly speaking), with all other parameters constant

$$\frac{\tau_{space}}{\tau_{earth}} \approx \left(\frac{g_{space}}{g_{earth}}\right)^{-\frac{1}{3}} \approx (10)^{\frac{1}{3}} \approx 30 \tag{13}$$

i.e., space provides an excellent opportunity to increase the yield of the grown crystals.

1.1.3 Application of Static Magnetic Fields

A less expensive way to modify convection is through the application of magnetic fields. The basic mechanism for the interaction of an applied magnetic field and a molten semiconductor involves the electrical currents induced by the movement of a conductor in the presence of a magnetic field. When convection is present, flow of this electrically conductive fluid perpendicular to the field results in a Lorentz force that opposes that motion. To determine the effectiveness of the magnetic field on the suppression of convection it is necessary to solve Maxwell's equations and the fluid flow equations for the velocity and electromagnetic fields. A complete derivation of the MHD equations is given in[9] and basically results in the incorporation of the Lorentz force

$$\vec{F}_{Lorentz} = \sigma(\vec{E} + \vec{V} \times \vec{B}) \times \vec{B} \tag{14}$$

into the Navier-Stokes equation (eq. 4). The neglection of the induced EMF $\vec{E}$ has been shown to be valid in the limit of two-dimensional flow.[10] With this approximation equation 14 reduces to

$$\vec{F}_{Lorentz} = \sigma(\vec{V} \times \vec{B}) \times \vec{B} \tag{15}$$

where σ is the electrical conductivity of the fluid, $\vec{V}$ is the fluid velocity vector and $\vec{B}$ determines the magnitude and orientation of the magnetic field. In many respects the damping of the convection by magnetic fields is similar to a change in the viscosity of the liquid. This has given rise to the term 'magnetic viscosity' which is analogous to the kinematic viscosity and is commonly denoted as

$$\nu_{magn} = \sigma\mu_0 \tag{16}$$

where μ_0 is the fluid permeability.

The nondimensional parameter which determines the effectiveness of the magnetic field on the suppression of convection is the Hartmann number, Ha,

$$Ha = BL\left(\frac{\sigma}{\mu}\right)^{\frac{1}{2}} \tag{17}$$

which is the ratio of the Lorentz force to the viscous force. For typical semiconductors and medium to large field strengths, $Ha \approx 10^6$, indicating that the electrical currents are better at transporting energy over larger distances in the melt than the viscous forces. Using a similar scaling argument as that presented above and noting,

$$\frac{\nu_{magn}}{\nu} \approx 10^6, \tag{18}$$

it can be shown that

$$\frac{\tau_{magn}}{\tau} \approx \left(\frac{\nu_{magn}}{\nu}\right)^{\frac{1}{3}} \approx 100. \tag{19}$$

Thus, both processing in microgravity and with the application of a magnetic field provide the potential to increase the quality and yield of semiconductor material.

This research focuses on the latter approach to suppress convection in a molten semiconductor. In the next section, a brief description of the experimental magnetic crystal growth system will be presented. Then we will discuss crystal growth results in a magnetic field. Direct comparisons will be made between microgravity and zero magnetic field cases.

2 Crystal Growth Apparatus

The ingots were grown by directional solidification in a vertical Bridgman-Stockbarger furnace. The furnace consisted of: a hot zone where the sample was melted; a booster heater located between the hot zone and gradient zone and a 0.3 cm heat extraction plate placed between the gradient and cold zone, which produced the high axial gradients necessary for this research. A guard heater was utilized on the end of the hot and cold zones to minimize any thermal losses out the end of the furnace. The furnace surface was maintained at 20 C with a water coolant loop. This furnace was designed to provide similar thermal environments as those produced by NASA's two microgravity furnaces, the Advanced Automated Directional Solidification Furnace (AADSF) and the Crystal Growth Furnace (CGF). The ampoule was supported by a cartridge assembly described in detail in.[11] This configuration was used during microgravity growth of $Hg_{0.8}Cd_{0.2}Te$ and was adapted for this research in order to have a direct comparison. Crystal growth was achieved by translating the furnace which allowed crystallization to take place in the homogenous region of the magnetic field. The furnace assembly was coaxially aligned with a superconducting magnet system designed specifically for this research[12] as shown in figure 2.

3 Experimental results and discussion

The effect of convection on segregation was determined by measuring radial and axial compositional variations. Before sectioning, surface morphology and axial compositional measurements were made on the as grown ingots. This data, along with growth orientation, was used to determine the sectioning of the ingot for further study.

For radial segregation measurements wafers were cut perpendicular to the growth direction. Axial segregation was determined from centerline samples cut parallel with the growth direction. The macrosegregation of CdTe was determined by Precision Density Measurements (PDM)[13] while microsegregation was determined from the transmission edge of the IR transmission spectrum and Energy Dispersive X-ray spectroscopy analysis (EDX).[14]

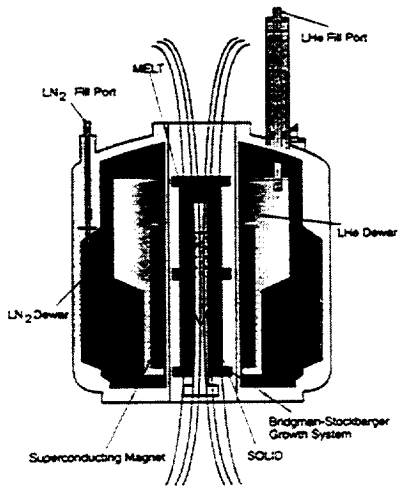

Figure 2: Schematic of superconducting magnet and crystal growth system.

3.1 Axial compositional distribution

For all growths with zero magnetic field the axial compositional profiles compared well with the profile predicted by the one-dimensional model by Clayton and colleagues[15] see figure 3. The axial compositional profiles for all growths under the influence of a magnetic field also compared well with the one-dimensional diffusion model with the exception of an abrupt compositional rise near the end of the ingot. This rise in composition has been attributed to constitutional supercooling and has been described in detail in.[11]

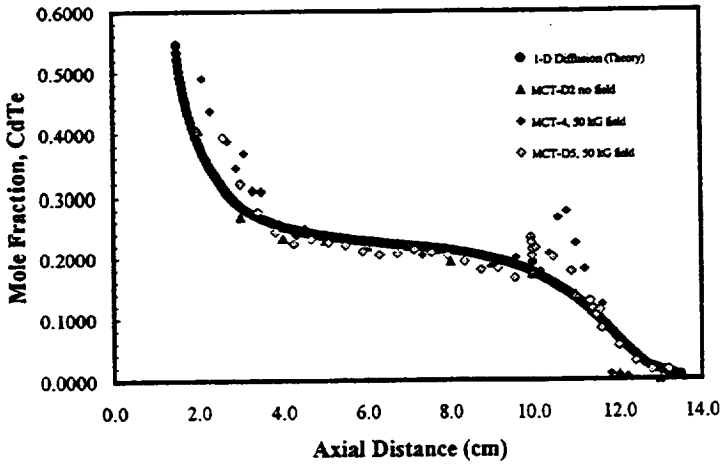

Figure 3: Comparison of experimental axial compositional distributions to one dimensional theory.

3.2 Radial compositional distribution

Radial compositional profiles for growth in 0, 5, 10 and 50 kG magnetic fields are shown in figure 4. All

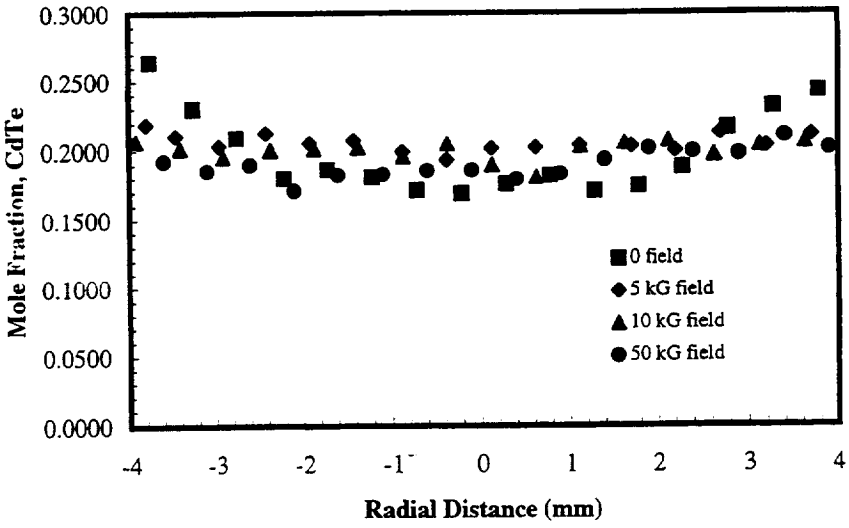

Figure 4: Radial compositional distributions.

wafers were taken at an axial position of 60 mm from the first to freeze portion of the as grown ingot. The pattern of low CdTe content at the center of the wafer for zero magnetic field is consistent with other results obtained previously in the absence of a magnetic field. This large radial compositional variation is consistent with a concave (toward the solid) interface curvature where the less dense component (HgTe) tends to accumulate at the lowest gravitational potential. There is a remarkable improvement in radial segregation in all samples grown in the magnetic field which indicates that reduction of convection through the application of a magnetic field is advantageous for maintaining the solid-liquid interface shape required to minimize the compositional variation transverse to the crystal growth direction.

To further investigate the effects of the magnetic field on interface shape, experiments were performed to mark the solid-liquid interface during growth with and without the influence of the stabilizing magnetic field. This was accomplished by quenching the sample after approximately 65 mm of growth. The resulting interfaces are shown in figure 5. The interface curvature for the crystal grown in a 50 kG field was a factor of three less than the interface obtained with zero field. This suggests that the convection has a significant influence on the interface morphology HgCdTe system. Information on the fluid flow velocities and fluid flow patterns are necessary to make definitive conclusions about the convective effects on interface morphology.

To estimate the relative magnitude of the convection in the HgCdTe system the analytical model for double-diffusive convection by Hart[16] was utilized. This model was originally developed to study salinity gradients but has been shown to be applicable to nondilute crystal growth systems.[17] Hart solves the linearized forms of equations 4, 7 and 8 in terms of a single solution parameter dependent only on the solutal Raleigh number, $M = (-0.25Ra_s)^{\frac{1}{4}}$. Using this analysis and the parameters for the HgCdTe system, the maximum velocity in the system without the magnetic field is 10 μm/sec. This is 5 times larger than the velocity required for diffusion limited growth (2 μm/sec) as determined from a $Pe_s \approx 1$ calculation and results in large convective interference with segregation. The maximum velocity during crystal growth with magnetic field is on the same order as the diffusion limited velocity and corresponding radial segregation is nearly uniform. It is of interest to note that if the flows in the HgCdTe system are indeed as slow as predicted by this analysis a smaller magnetic field should still produce uniform radial segregation. To this end, growths with magnetic field strengths of 10 and 5 kG

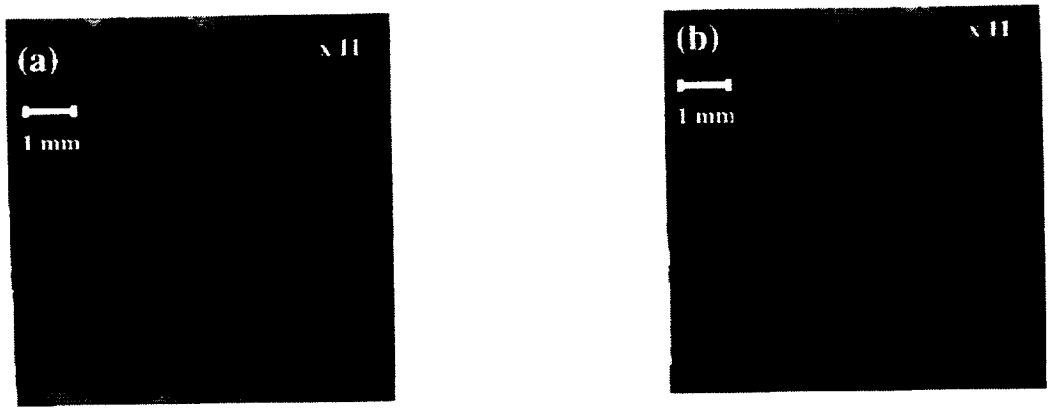

Figure 5: Solid-liquid interface shapes for growth (a) zero magnetic field, (b) 50 kG magnetic field.

were performed. This represents an order of magnitude change in field strength and in all cases uniform radial segregation was obtained as shown in figure 4.

To further quantify the effects of the magnetic field on the radial segregation, the experimental results were compared to the analysis of the lateral solute segregation associated with a curved solid-liquid interface during steady-state unidirectional solidification of a binary alloy as derived by Coriell and Sekerka.[18] Briefly, they solved the species continuity equation for the radial solute concentration in the solid crystal at the solid-liquid interface with the assumptions of no convection in the liquid and that the solid-liquid interface could be represented by a Fourier series. Their work showed that in the limiting case (i.e., when the solute boundary layer is thick compared to the deviation of the solid-liquid interface from planarity), the transverse segregation in the solid is proportional to the deviation of the interface from planarity, the proportionally factor being just the product of the unperturbed concentration gradient and the distribution coefficient. The Coriell formalism is developed for a 2-D rectangular geometry which does not completely describe the crystal growth geometry in the HgCdTe system. To rectify this problem a numerical code based on the Coriell formalism was developed to predict radial compositional distributions in HgCdTe. The configuration used was a cylindrical system at steady state growth conditions and the solid-liquid interface was expressed in terms of a series combination of Bessel's functions. The details of this analysis are described in detail elsewhere.[19] These calculations are applicable for crystal growth in a stabilizing magnetic field where the field strength is sufficient to suppress convection. The radial segregation for growth in a 50 kG magnetic field is shown in figure 6. There is excellent agreement with the Coriell formalism and indicates that the radial segregation is approaching the diffusion limited regime.

4 Comparison with microgravity crystal growth results

A $Hg_{0.8}Cd_{0.2}Te$ alloy crystal was grown in the microgravity environment aboard the space shuttle during the Second United States Microgravity Mission in March 1994. The grown ingot was approximately 16 cm long and 0.72 cm in diameter. During the mission portions of ingot were grown while the orbiter was in different attitudes. The influence of orbiter attitude and, hence, the residual drag acceleration on the growth process was investigated by examining the radial composition of the ingot during the +YVV/-ZLV and -ZVV/-XLV portions

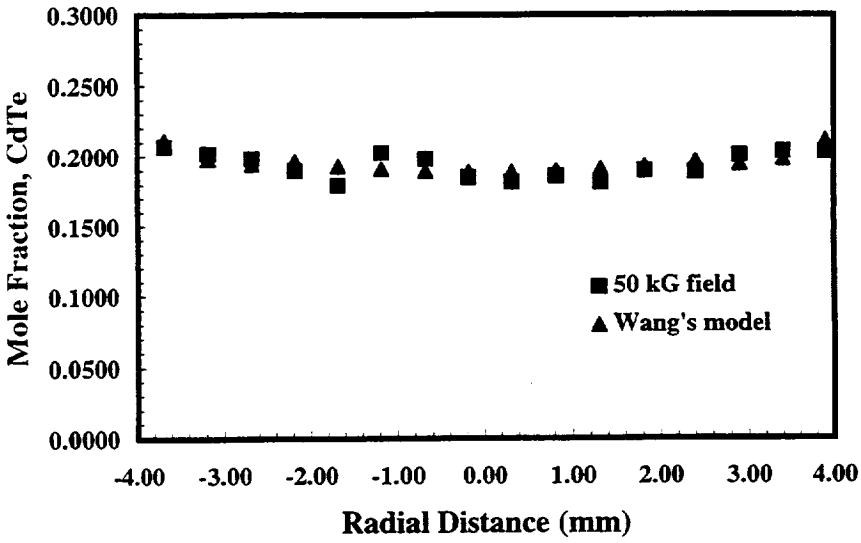

Figure 6: Comparison of radial compositional profile obtained with the application of a 50 kG magnetic field to theory.

of the mission see figure 7.

The radial compositional profiles for the different attitudes are shown in figure 8. These measurements were taken at 15 degree intervals at circumferences within the sample at progressively increasing distances from the edge, and starting at 100 μm in. As can be seen, the asymmetry in the compositional variation across the 63 mm wafer shows a definite correlation with the direction of the residual acceleration vector resolved on this plane. This is attributed to residual fluid flow. This growth configuration is unstable in that there is a residual acceleration component in the direction of solid to liquid, which is destabilizing. In similar vein, the sample cut at 106 mm also shows asymmetry, and once again the effect of the residual acceleration component is to affect the distribution of the liquid such that the heavier material is sedimented asymmetrically by the residual force. In this part of the growth, there was a stabilizing vector, albeit small, in the direction of liquid to solid. This contrasts with the 63 mm wafer, and has resulted in a more homogeneous wafer. The compositional profile for growth in a 50 kG magnetic field is shown in figure 8c. The compositional distribution is more uniform and symmetric which indicates that the magnetic field is efficacious in suppressing convection that may result from any misalignment with the gravity vector under 1g conditions.

5 Summary

To summarize, the most interesting finding of this research is that convective interference with segregation and the interface morphology in the HgCdTe system is quite subtle. By reducing fluid flow from 10μm/sec (no magnetic field) to 2μm/sec (magnetic field), the solid-liquid interface deviation from planarity was reduced by a factor of 3. This is attributed to the large separation of the liquidus and solidus phases in the HgCdTe system which produces a highly compositional dependent solid-liquid interface. The importance of the solutal term compared to the thermal term on density should be noted. A change of 5 to 10 percent in composition

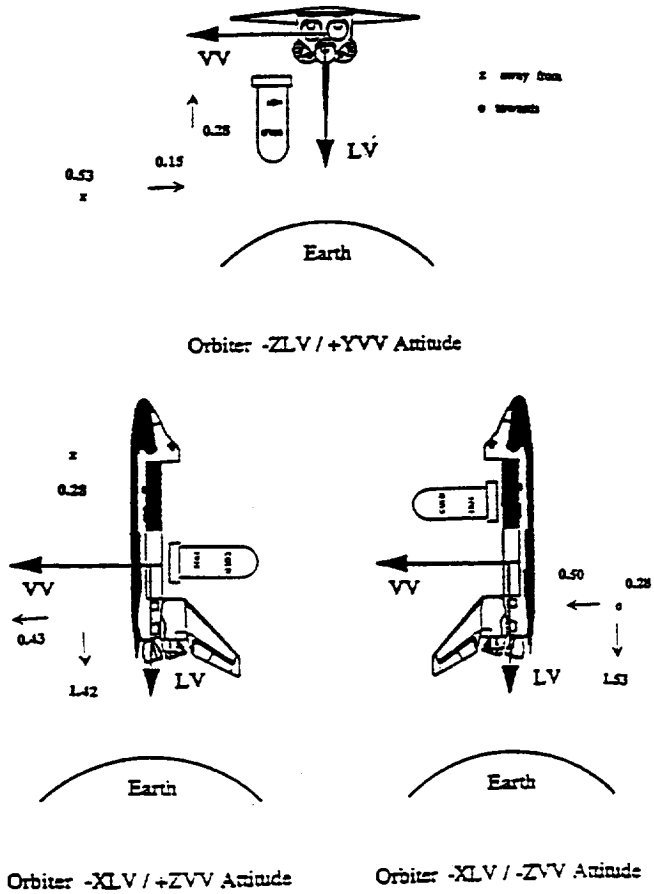

Figure 7: Components of residual acceleration at AADSF during USMP-2.

has the same effect on density as a 150 C change in temperature. Therefore, a small reduction in fluid flow (i.e., reducing the build-up of the solute at the sample center) will tend to produce a more planer solid-liquid interface. Obviously, one can never achieve a planer interface due to the differences of thermal conductivities of the melt, solid and containing crucible. However, this effect can be minimized by judiciously choosing the thermal boundary conditions.

In microgravity crystal growth a strong correlation between the relative magnitude and orientation of the residual acceleration due to drag was observed. If the drag vector is not aligned parallel to the growth direction (liquid to solid) three dimensional fluid flow will result which destroys the symmetry of the system and leads to nonuniform radial segregation.

6 Acknowledgments

The authors wish to thank Curtis Bahr, Rens Ross and Don Lovell who are members of the Engineering Support Staff at the Marshall Space Flight Center. Without their uncompromising efforts, cooperation and enthusiastic support this project would not of been successful.

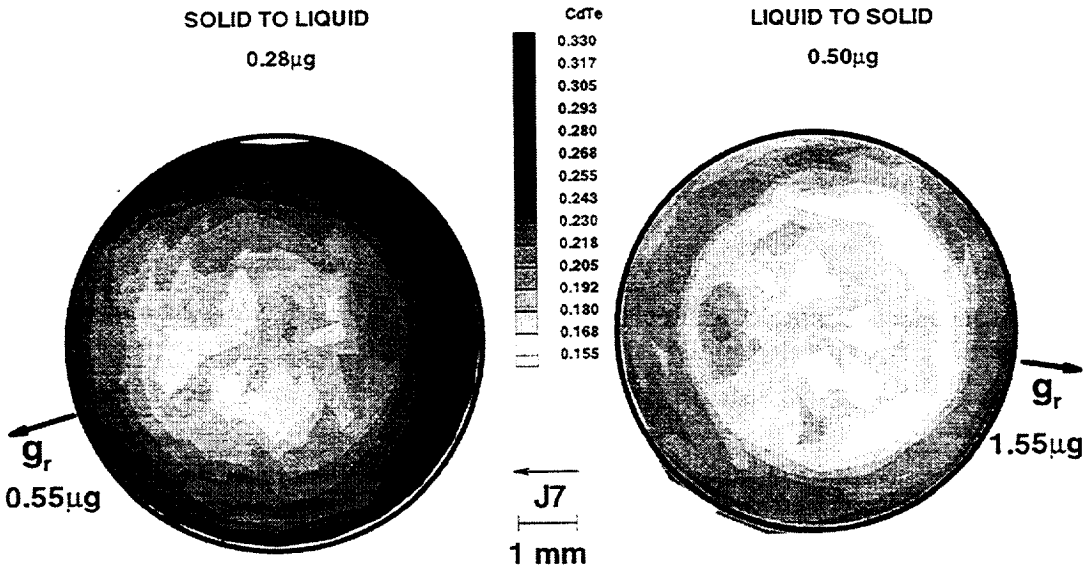

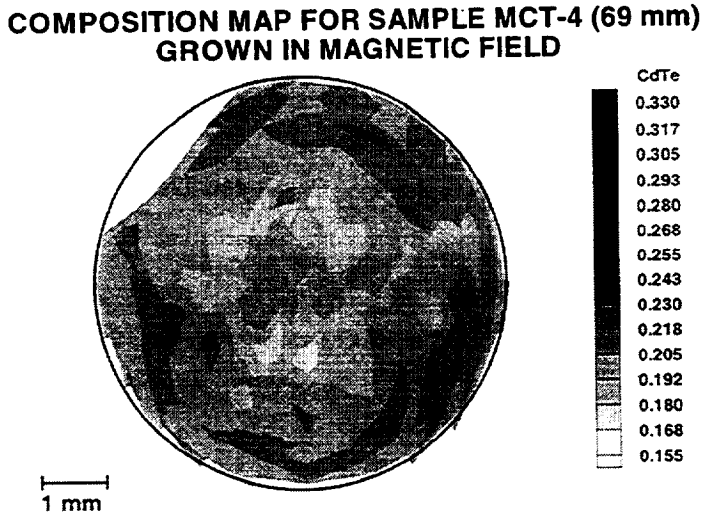

Figure 8: (a) Radial compositional map for the +YVV/-ZLV attitude (63 mm), (b) radial compositional map for the -ZVV/-XLV attitude (106 mm), (c) radial compositional map for a sample grown in a 50 kG magnetic field (69 mm).

7 REFERENCES

[1] T. Jasinski and A.F. Witt, J. Crystal Growth 71 (1985) 295.

[2] D.E. Holmes and H.C. Gatos, J. Electrochem. Soc., 128 (1981) 429.

[3] A.F. Witt in Porceedings Third Space Processing Symposium, Skylab results: Volume 1, NASA-Marshall Space Flight Center, June (1974).

[4] Instruction Manual for Superconducting Magnet, Cryomagnetics, Inc., Oak Ridge, TN.

[5] H.C. Gatos in Summary Science Report, Apollo-Soyuz Test Project Volume 1, NASA-Johnson Space Flight Center, NASA SP-142, Washington DC (1977).

[6] J.L. Reger in Proceedings Third Space Processing Symposium, Skylab results: Volume 1, NASA-Marshall Space Flight Center, June (1947).

[7] H. Wiedemeier, F.C. Klaessig, S.J. Wey and E.A. Irene in Proceedings Third Space Processing Symposium, Skylab results: Volume 1, NASA-Marshall Space Flight Center, June (1974).

[8] D.J. Larson, Jr., J.I.D. Alexander, D. Gillies, F.M. Carlson, J.Wu and D. Black, NASA Conference Publication 3272, Launch +one year Science Review of USML-1, 1994.

[9] S. Chandrasekhar, Phil. Mag. Ser. 7, Vol. 43 (1952) 501.

[10] J. Baumgartl and G. Muller, Proc. 8th European Symp. on Materials and Fluid Science in Microgravity, Brussels (1992). ESA Publication no SP. 333.

[11] D.A. Watring, S.L. Lehoczky, J. of Crystal Grówth, To be published.

[12] Instruction Manual for Superconducting Magnet, Cryomagnetics, Inc., Oak Ridge, TN.

[13] H.A. Bowman and R.M. Schoonover, J. of Research National Bureau of Standards Vol. 71C (1967) 179.

[14] D.C. Gillies, J. Electron. Mater. 11 (1982) 689.

[15] J.C. Clayton, M.C. Davidson, D.C. Gillies and S.L. Lehoczky, J. of Crystal Growth 60 (1982) 374.

[16] J. Hart, J. Fluid Mechanics (1969), Vol. 38 Part 2, 375.

[17] A. Rouzaud, D. Camel and J.J. Favier, J. of Crystal Growth 73 (1985) 149-166.

[18] S. Coriell and R. Sekerka, J. of Crystal Growth 46 (1979) 479.

[19] J.C. Wang, D.A. Watring and S.L. Lehoczky, in press.